第 XX 卷第 XX 期
XXXX 年 XX 月

红 外 与 毫 米 波 学 报
J. Infrared Millim. Waves

Vol. XX, No. XX
XX,XXXX

文章编号：1001-9014(XXXX)XX-0001-09

DOI:10. 11972/j. issn. 1001-9014. XXXX. XX. 001

A broadband terahertz quasi-optical detector based on 3D-printed lens packaging

WANG Bing[1]， LI Ming-Xun[2*]， LV Xin[1]

（1. Beijing Key Laboratory of Millimeter Wave and Terahertz Technology, School of Integrated Circuiits and Electronics, Beijing Institute of Technology, Beijing 100081, China;
2. Beijing Altos Radar CO., LTD., Beijing 100095, China）

Abstract: A broadband terahertz (THz) quasi-optical detector based on 3D-printed lens packaging has been presented, covering two typical atmospheric windows at 220 GHz and 340 GHz. The detector consists of an antenna-coupled detector chip and a 3D-printed lens. The antenna-coupled detector chip was packaged on the multi-layer dielectric laminate with the Schottky diode directly integrated across feeding terminals of the chip-on antenna. Patterns of the on-chip integrated broadband planar bowtie antenna were printed on a quartz substrate within the operation frequency range of 201-360 GHz, serving as a radiator and a radio frequency (RF) choke. It utilized a pair of capacitively loaded loop (CLL) to broaden the operational bandwidth, while essentially maintaining the overall antenna dimensions. Additionally, well-designed high-impedance folded low-frequency (LF) leads were integrated for achieving effective signal isolation and radiation coupling characteristics. To achieve unidirectional antenna radiation patterns and enhance the overall structural mechanical robustness, a lightweight and lost-cost 3D-printed lens combined with metallized reflector buried in multi-layer dielectric laminate was proposed. The detector exhibits a maximum voltage responsivity of 2200 V/W in the 200-230 GHz range, and 1885 V/W in the 320-350 GHz range. The measured radiation patterns show good agreement with the simulated results.

Key words: terahertz (THz) quasi-optical detector, broadband, integrated bowtie antenna, 3D-printed lens, Schottky diode

PACS:

一种基于3D打印透镜封装的宽带太赫兹准光探测器

王 兵[1]， 李明迅[2*]， 吕 昕[1]

（1. 北京理工大学 集成电路与电子 毫米波与太赫兹技术北京市重点实验室，北京 100081；
2. 北京傲图科技有限公司，北京 100095）

摘要：本文提出了一种基于3D打印透镜封装的宽带太赫兹(THz)准光探测器，可覆盖220 GHz和340 GHz两个典型大气窗口．该探测器由天线耦合探测芯片和3D打印透镜组成．天线耦合探测芯片通过多层介质衬底封装，肖特基二极管直接集成在片上天线的馈电端口．片上集成的平面蝶形天线图案刻蚀在石英基底上，工作频率范围为201－360 GHz，兼具辐射器与射频(RF)扼流的功能．该天线引入容性负载环路(CLL)以拓展工作带宽，同时基本保持整体尺寸不变．此外，设计了高阻抗折叠的低频(LF)引线，以实现有效的信号隔离和辐射耦合特性．提出了一种低成本，轻量化的3D打印透镜，该透镜与埋置于多层介质层压板中的金属化反射器相结合，实现天线定向辐射并增强整体结构的机械稳定性．该探测器在200－230 GHz范围内的最大电压响应度为2200 V/W，在320－350 GHz范围内的最大电压响应度为1885 V/W，实测辐射方向图与仿真结果表现出较好的一致性．

关 键 词：太赫兹(THz)准光探测器；宽带；集成化蝶形天线；3D打印透镜；肖特基二极管

Foundation items: Supported by the Natural Science Foundation of China (61527805)

Biography: Wang Bing (1991—), male, Henan China. Ph. D. Research area involves terahertz device and terahertz imaging. E-mail: wangbingbit0726@163.com

[*] **Corresponding author**: mingxunli@altosradar.com

Introduction

Wireless communications[1-2], remote sensing[2-3] and imaging[4-6] are arguably the most important applications of terahertz (THz) technology. In recent years, the rapidly growing demands for higher data-rate communications and high-resolution imaging have driven wireless systems toward increasingly broader operational bandwidths. The THz detector constitutes a key component of the receiver front end, that directly determines receiver performance in the absence of a low-noise amplifier. Generally, THz detectors can be classified into two categories: waveguide-based detector with a horn antenna and antenna-coupled detector, namely quasi-optical detector. Compared with the waveguide-based one, the quasi-optical detector provides several advantages, including broader bandwidth, reduced size, lighter and easier fabrication[7-9]. Additionally, it can be much less expensive in large quantities, and flexibly configured into a miniaturized 2-D array.

To achieve broadband performance, THz quasi-optical detectors typically employ planar thin-film antennas with log-periodic[10] or spiral geometries[11-12], which exhibit stable radiation characteristics across wide frequency ranges. However, such complementary antenna elements generally feature complex geometries, imposing stringent requirements on fabrication processes. Therefore, it is desirable to adopt a structure that is easily fabricated and robust against minor fabrication tolerances. In addition, a silicon lens is usually utilized to enhance the antenna gain, which substantially increases the overall cost [8-9]. Moreover, when scaling up to large detector arrays, the use of silicon lens introduces considerable signal transmission losses and complicates the system assembly.

In this paper, we proposed a broadband and lightweight THz quasi-optical detector, that operates over 201 – 360 GHz covering two typical atmospheric windows at 220 GHz and 340 GHz. Two major contributions in the work are highlighted here: 1) a broadband chip-on bowtie antenna with a pair of capacitive loop load (CLL) is proposed for THz Schottky diode-based detector. The operation principle of the antenna was clarified through the equivalent circuit of the antenna-coupled detector, and detailed simulation analyses were performed to achieve high coupling efficiency within the full operational bandwidth. 2) a 3D-printed nylon lens, integrated with a buried metallized reflector, was designed to achieve unidirectional radiation patterns and enhanced antenna gain, resulting in a low-cost and lightweight detector package. The detector prototype was fabricated, packaged, and experimentally characterized. The measurement results shows that the voltage responsivity is 1025-2200 V/W in the 200-230 GHz range, and 1033-1885 V/W in the 320-350 GHz range, demonstrating the feasibility of the proposed broadband detector.

1 Design of the quasi-optical detector

1.1 Package stack-up and design concept

Fig. 1 shows the geometry of the THz quasi-optical detector. It adopts a hybrid dielectric substrate configuration. From the top to bottom, it consists of an extended hemispherical nylon lens, a quartz substrate (relative permittivity: 3.78) and multi-layer printed-circuit-board (PCB). The nylon has a low relative permittivity of 2.64, which helps to minimize the effect of interface reflection caused by large difference in relative permittivity. Besides, the lens is realized via 3D-printed technology, facilitating the implementation of a cost-effective and lightweight. To suppress surface wave excitation at the THz bands, the quartz substrate has thin thickness of 50 μm. The multi-layer PCB consists of two dielectric laminates and a metal layer as the planar reflector, which enhances the structural strength by increasing the total thickness of the substrates. Here to achieve a broadband and high-efficiency antenna, a Rogers 5880 substrate (relative permittivity: 2.2) is chosen as one laminate, while a cost-effective Rogers 4350B substrate (relative permittivity: 3.66) is adopted as the other.

The pattern of the antenna-coupled detector chip is defined on a quartz substrate as shown in Fig. 1(d), which contains an on-chip bowtie antenna and a Schottky diode (SBD). The SBD, acting as the detecting element, is directly integrated across the feeding terminal of the antenna. The bowtie antenna is comprised of a pair of CLL adjacent to the central terminal and folded high-impedance lines at the ends of the two antenna arms. The two CLLs are symmetrically placed with their openings facing the central terminal of the antenna. The folded high-impedance lines are wire-bonded to the PCB, functioning as low-frequency (LF) leads to extract the detected signal. The signal is subsequently routed through a signal via to the output port, while a ground via connects to the metallized reflector.

Additionally, the 3D printing lens, integrated above the on-chip antenna, plays a significant role in enabling the bowtie antenna to generate unidirectional RF radiation with enhanced directivity and gain. To ensure reliable operation and protection, a cylindrical air cavity is incorporated at the bottom of the lens, providing a hermetic package for the antenna-coupled detector.

1.2 on-chip bowtie antenna and equivalent circuit model

Fig. 2 shows the details of the integrated on-chip bowtie antenna. It comprises an antenna element and LF leads, which are used to receive radio-frequency (RF) signal from free space and route the detection output, respectively. The Schottky is replaced by a lumped port with 50 Ω[13]. The main body of antenna element is differential bowtie structure, whose width is gradually widened following:

$$w(t) = W\exp\left[k(t - L/2)\right] \tag{1}$$

Where W is the width of the central terminal, L is the spacing between central terminal, and k is the gradient factor of the exponential edges.

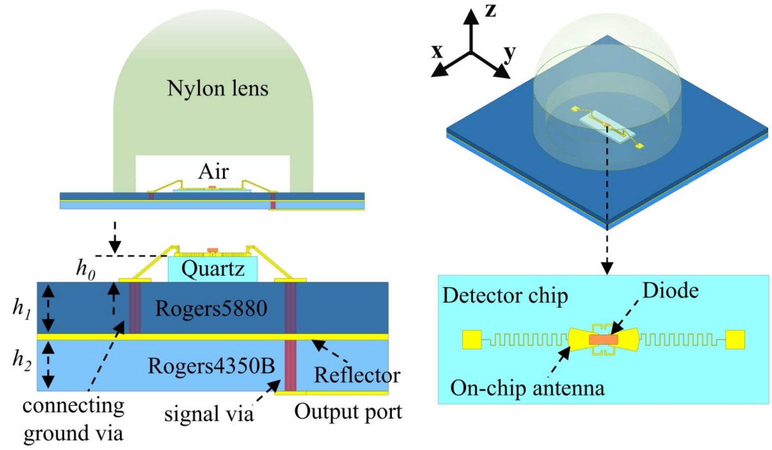

Fig. 1　The geometry of the THz quasi-optical detector (Design parameters: h_0=50 μm, h_1=0. 127 mm, h_2=0. 1mm)
图1　太赫兹准光探测器的几何形状(设计参数:h0=50 μm, h1=0. 127 mm, h2=0. 1mm)

The length of the main body *L2* is approximately set as $\lambda_L/4$, where λ_L is the wavelength at the lower resonance frequency. The exponential edges can facilitate a smoother impedance transition. However, they will result in excessively wide ends, leading to a significant discontinuity between the antenna element and LF lead. To mitigate this mismatch and suppress higher-order modes, the four corners of main body are rounded with a radius of *Ra*. Besides, the rounded corners promote smoother current flow and increase the equivalent electrical length, effectively lowering the fundamental resonance frequency. Consequently, the physical length of the main body can be reduced while maintaining the desired resonance characteristics.

To further enhance the bandwidth of the bowtie antenna, two symmetrical split-ring resonators are positioned near the central terminal of main body, forming additional resonant loops that act as CLLs and introduce new resonance frequency[14-16]. Moreover, when the split-ring resonators are placed face-to-face, an additional transmission zero is generated through their electric coupling, which further improving the antenna's operational bandwidth[17]. Fig. 3 presents the simulated |S11| of the main body with and without CLLs. The results clearly demonstrate that the incorporation of CLLs leads to a substantial enhancement in bandwidth, expanding from 25% to 64%.

It is noteworthy that the LF leads alter the impedance characteristics of the antenna element, which may significantly deteriorate its overall performance. To mitigate this effect, effective isolation between the RF and LF signals is essential. Accordingly, the LF leads are designed as folded high-impedance transmission lines to achieve sufficient signal isolation.

To clarify the operating mechanism of the integrated broadband bowtie antenna for detector, the equivalent circuit model of antenna-coupled detector is presented in Fig. 4. The circuit comprises two distinct signal paths, where the blue and green loops represent the RF and LF paths, respectively. The incident RF radiation is coupled by the integrated bowtie antenna and converted into RF current, which will then be detected by SBD and output at the bottom of multi-layer PCB.

The integrated bowtie antenna is equivalent to a series connection of a differentially fed antenna and a pair of inductors at two sides in the circuit. In the RF path, the differential antenna serves as a radiator for receiving RF signal from free space, but behaves as a non-radiating transmission line in the LF path.

The CLLs are loaded in parallel with the bowtie antenna, while the TT′plane perpendicular to the electric field direction of the bowtie antenna acts as PEC boundary. The resonant circuit model of CLL is illustrated within the green dashed box. The L and C represent the in-

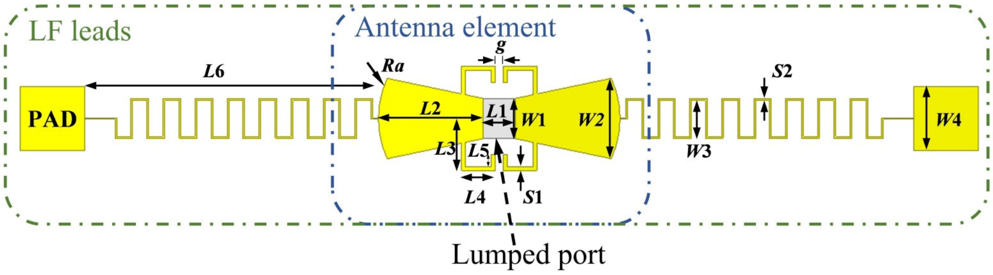

Fig. 2　The details of the on-chip integrated bowtie antenna (Design parameters: *L1*=40 μm, *L2*=131 μm, , *L3*=65 μm, *L4*=42 μm, *L5*=20 μm, *L6*=360 μm, *W1*=50 μm, *W2*= 100 μm, *S1*=5 μm, *Ra*=120 μm, *g*=10 μm)
图2　片上集成蝶形天线的具体结构(设计参数:L1=40 μm, L2=131 μm, , L3=65 μm, L4=42 μm, L5=20 μm, L6=360 μm, W1=50 μm, W2= 100 μm, S1=5 μm, Ra=120 μm, g=10 μm)

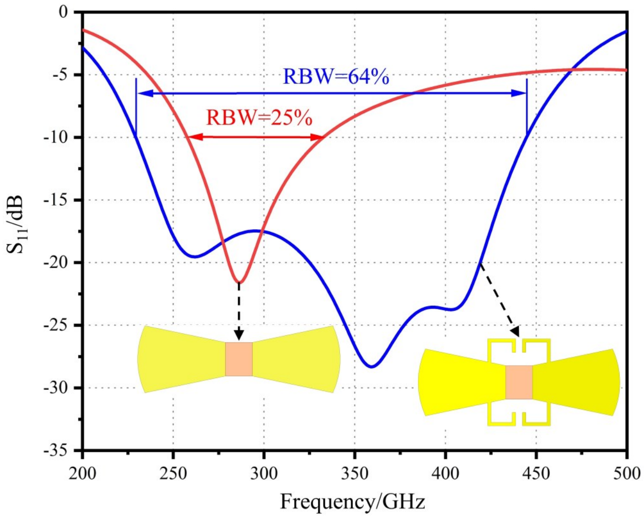

Fig. 3 Simulated reflection coefficients of the bowtie antenna with and without CLLs
图3 在有无CLL条件下蝶形天线反射系数仿真结果

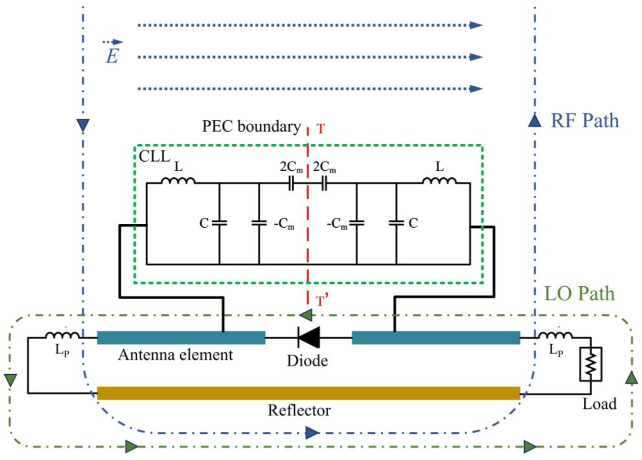

Fig. 4 The equivalent circuit model of antenna-coupled detector
图4 天线耦合探测器的等效电路模型

trinsic inductance and capacitance of the CLL, whereas C_m denotes the equivalent capacitance arising from the coupling between the two CLLs.

Accordingly, the resonant frequency of the two electrically coupled CLLs can be expressed as:

$$f = \frac{1}{2\pi\sqrt{L(C + C_m)}} \tag{2}$$

It can be seen that the resonant frequency f is primarily determined by the effective electrical length of the two CLLs and the spacing g between them. Therefore, by adjusting the CLLs length and the coupling degree, the antenna bandwidth can be flexibly tuned while preserving the overall dimensions of the bowtie antenna. To clarify this, a group of simulated |S11| of the antenna with different values of g is plotted in Fig. 5.

The simulation results indicate that variations in the spacing between the two CLLs have little effect on resonant frequency of the bowtie antenna. However, as the spacing increases, the slanted edges of the bow-tie antenna lead to an expansion of its effective width, thereby reducing the effective electrical length of the CLL. Consequently, the intrinsic resonant frequency of the CLL shifts toward higher values. Moreover, the increased spacing weakens the coupling between the two CLLs, which is consistent with the elevated reflection coefficients observed in the simulations. Considering both the effects of dimensional variation on the resonant frequency and the coupling strength, the spacing between the two CLLs is chosen to be 10 μm.

To reduce the impact of LF loading on the antenna's impedance matching, the LF leads are implemented as folded high-impedance transmission lines, that block RF current while allowing LF current to pass. In the equivalent circuit model, the LF leads are represented by inductance L_p and assigned to the LF signal path. Addition-

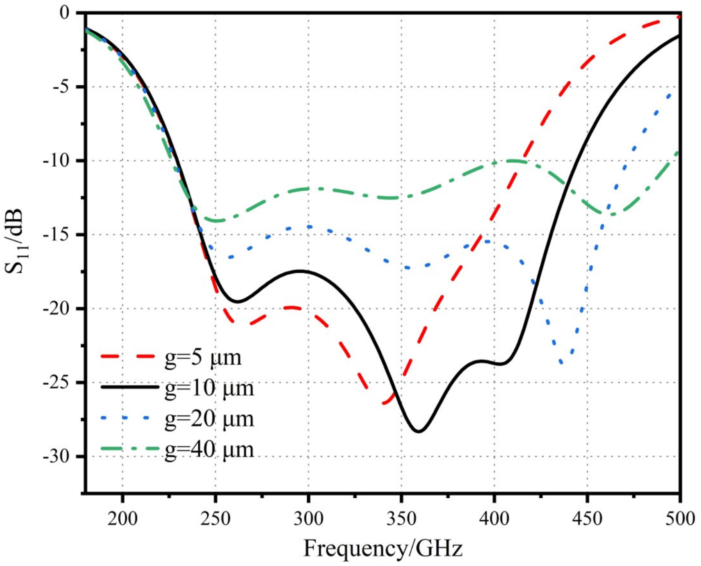

Fig. 5 Simulated reflection coefficients of the bowtie antenna with different values of g
图5 不同g参数取值条件下蝶形天线反射系数仿真结果

ally, the planar reflector under the bowtie antenna serves as an impedance tuner for the RF path and a ground plane for the LF signal.

Fig. 6 presents a comparison of the simulated |S11| for the broadband bowtie antenna with and without the LF leads. It is observed that the introduction of folded LF leads shift the bowtie antenna's operating frequency toward lower values, but has minimal influence on the coupling strength and relative bandwidth. The resulting broadband antenna achieves an impedance bandwidth of 201 – 405 GHz with a relative bandwidth of 67%, effectively covering two typical atmospheric windows at 220 GHz and 340 GHz.

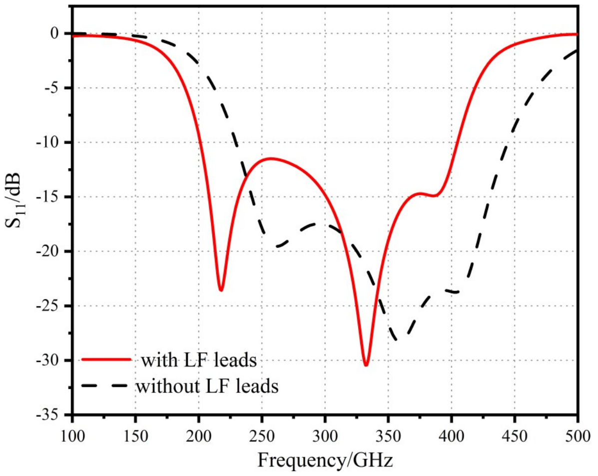

Fig. 6 Simulated reflection coefficients of the bowtie antenna with and without the LF leads
图6 在有无低频引线条件下蝶形天线反射系数仿真结果

1.3 3D-printed lens antenna

For generating highly directional beam for effectively coupling the incoming RF radiation, an extended hemispherical lens is loaded upon the bowtie antenna and mounted on the front side of the PCB. To maximize coupling efficiency of the lens antenna, a low-permittivity nylon material was selected. Considering both cost and fabrication reliability, the lens was fabricated using 3D printing, a promising technique that enables rapid production at low cost while maintaining high dimensional accuracy[18-19]. Furthermore, an air cavity was incorporated into the lens to prevent direct contact with the antenna-coupled detector, thereby mitigating the risk of damage, while simultaneously shortening the focal and extension lengths. This design also enhances focusing capability and increases the beam deviation angle compared with conventional dielectric lenses, contributing to a more compact and efficient lens antenna.

The geometry of 3D-printed lens consists of a hemispherical, an extended cylinder , and a cylindrical air cavity as shown in Fig. 7. The radius r of lens should ensure that the lens surface is located in the far field of the planar bowtie antenna. According to the Gaussian optics theory, the Gaussian field inside the lens would continue to propagate and focus on the waist position. The bowtie antenna, serving as the feeder, should be placed at the waist position of the Gaussian beam to maximize the coupling efficiency of antenna. Moreover, the size of the Gaussian waist is dependent on the operating frequency and the geometry of lens. For the purpose, we chose 10 mm as the lens's diameter. Based on the method in Ref. [20], we can estimate the corresponding geometric sizes and build original lens model. Then the MLFMA algorithm was applied to substitute geometrical optics method for the calculation of electromagnetic field distribution for achieving optimal the radiation patterns.

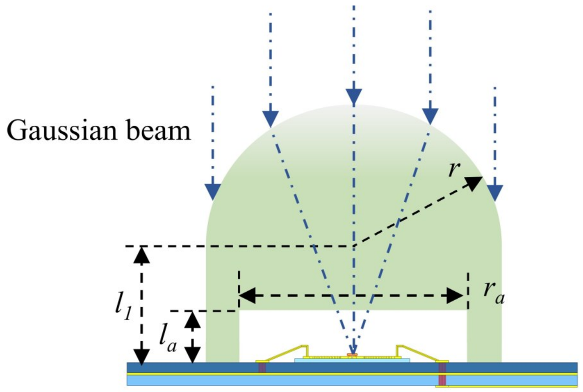

Fig. 7 The geometry of 3D-printed nylon lens (Design parameters: r=5 mm, l_1=3.5 mm, r_a=3 mm, l_a=1.8 mm)
图7 3D打印尼龙透镜几何形状(设计参数:r=5 mm, l1=3.5 mm, ra=3 mm, la=1.8 mm)

Fig. 8 presents the simulated radiation patterns of the bowtie antenna with and without the extended hemispherical lens. By introducing the lens, the planar antenna effectively achieves a larger radiating aperture, resulting in a significantly narrower beamwidth. At 220 GHz, the realized gain reaches 21 dBi, representing an improvement of 13.9 dBi compared with the lens-free planar antenna, while at 340 GHz, the realized gain increases to 22.3 dBi, corresponding to a 15 dBi enhancement.

As shown in Fig. 9, the lens antenna exhibits a 3-dB gain bandwidth of 150 – 360 GHz, representing an approximate 12% downward shift relative to the 201 – 405 GHz impedance bandwidth. Despite this shift, the antenna still effectively covers the 220 GHz and 340 GHz atmospheric windows, demonstrating its suitability for THz applications that demand broadband operation with high directivity.

2 Detector fabrication and measurement

2.1 Detector implementation and experiment

Based on the designed planar on-chip bowtie antenna, a broadband quasi-optical detector was fabricated and packaged. Fig. 10 shows a micrograph of the fabricated quasi-optical detector chip, which includes the bowtie antenna with the electromagnetically coupled CLLs for broadband, folded high-impedance transmission lines, pads and SBD. The bowtie antenna and circuits with 200-

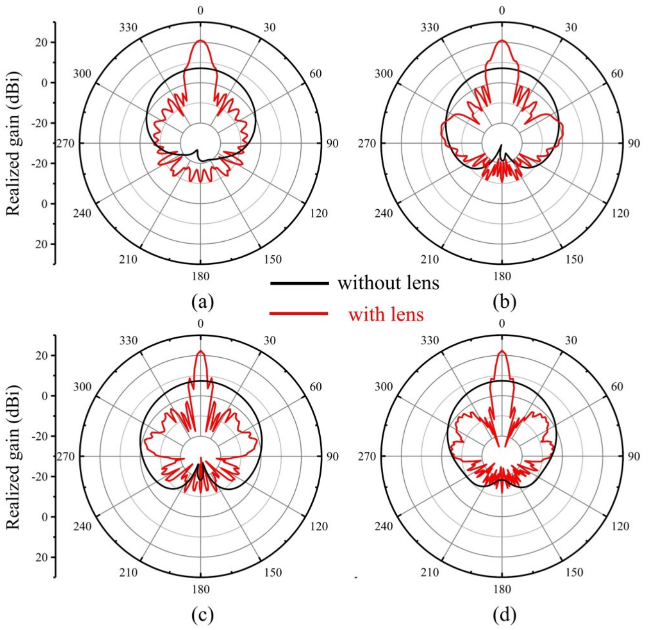

Fig. 8 Simulated radiation patterns of the bowtie antenna at (a) 220 GHz, E-plane, :(b) 220 GHz, H-plane, (c) 340 GHz, E-plane, (d) 340 GHz, H-plane(b) 220 GHz, H-plane, (c) 340 GHz, E-plane, (d) 340 GHz, H-plane

图8 蝶形天线在不同频率和平面下的仿真方向图 (a) 220 GHz, E-plane,

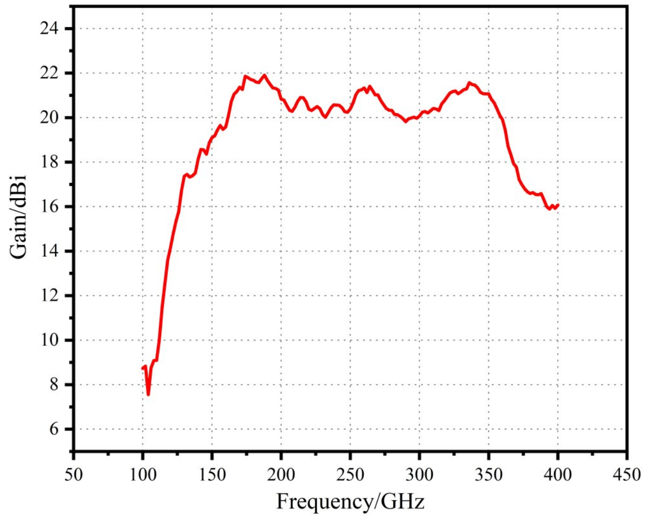

Fig. 9 Simulated gain of the lens antenna

图9 透镜天线仿真增益

nm-thick gold thin film was deposited on the 50-μm-thick quartz substrate by semiconductor photolithography technology. The SBD is flip chip attached across the central gap of the bowtie antenna by using the sliver epoxy. Known from the manufacturer, the critical parameters is as follows: serial resistance R_s=6 Ω, zero-biased junction capacitance C_{j0}=1. 16 fF, reverse saturation current I_s =9 fA, ideality factor n=1. 21. The whole dimensions of the diode are the length 280 μm, width 95 μm and thickness 35 μm. The total planar size of the quasi-optical detector is 0. 4λ_0×0. 96λ_0, where λ_0 is free-space wavelength. As shown in the inset of Fig. 11, the detector chip was packaged into a well-designed metal house as a module, and a 3D-printed nylon lens is loaded upon the front side of the chip. To ensure that the bowtie antenna is accurately positioned at the center of the nylon lens, alignment marks are patterned on the alumina chip, limiting the alignment tolerance to within 100 μm.

The schematic diagram of the detecting measurement setup is utilized to characterize the responsivity and radiation patterns of the quasi-optical detector, as shown in Fig. 11. The RF source consists of an 8257D signal generator and a ×24 multiplication chain, providing a continuous output of 20 mW at room temperature. A standard transmitting horn with a gain of 20 dBi is positioned in line-of-sight with the detector at a distance of 40 cm, satisfying the far-field condition. The fabricated detector under test is mounted on an electrically controlled positioning and rotating stage. A 100 kHz sinewave signal from a lock-in amplifier (SR850) is fed into the signal generator to generate an amplitude-modulated THz signal. A bias tee integrated on the LF port and DC current is provided by a dc supply.

2. 2 Radiation pattern

Due to the lens antenna is integrated with the Schottky diode, it is generally quite difficult to directly measure the radiation patterns of the RF antenna. It can be demonstrated in terms of the output voltage V_{out} recorded from the lock-in amplifier the rotation stage. Fig. 12 shows the normalized radiating patterns of the lens antenna on the E- and H-planes at 220 and 340 GHz. It can be found that a good agreement is achieved between the measurement and simulation on the pattern main lobes. Since the power level in the backside and cross-polarized direction is quite weak, only radiation patterns in the copolarized direction are measured.

2. 3 Responsivity

The responsivity R_v of the broadband quasi-optical detector is characterized by $R_v=V_{\mathrm{out}}/P_{\mathrm{RF}}$, with P_{RF} the incident RF power, which is evaluated based on Friis transmission equation as follows:

$$P_{RF}=\left(\frac{P_TG_T}{4\pi d^2}\right)\cdot\frac{G_R\lambda^2}{4\pi} \qquad (3)$$

Where λ is the free-space wavelength, P_T is the output power of the RF multiplier-chain module, G_T is the realized gain of the RF transmitting horn antenna, and G_R is the realized gain of the detector antenna obtained from the simulated results of the antenna. Fig. 13 shows the simulated responsivity of the quasi-optical detector versus RF frequency, which ranges between 1050 and 2100 V/W from 201 to 360 GHz. However, owing to the absence of a broadband terahertz source in the laboratory, the broadband quasi-optical detector was measured only at frequencies around 220 GHz and 340 GHz in Fig. 13, which correspond to the well-known atmospheric transmission windows in the terahertz regime. The measured responsivity ranges between 1025 and 2200 V/W from 200 to 230 GHz, and 1033 and 1885 V/W from 320 to 350 GHz. It is worth noting that the oscillations observed in the measured responsivity are primarily attributed to impedance mismatching between the diode and the anten-

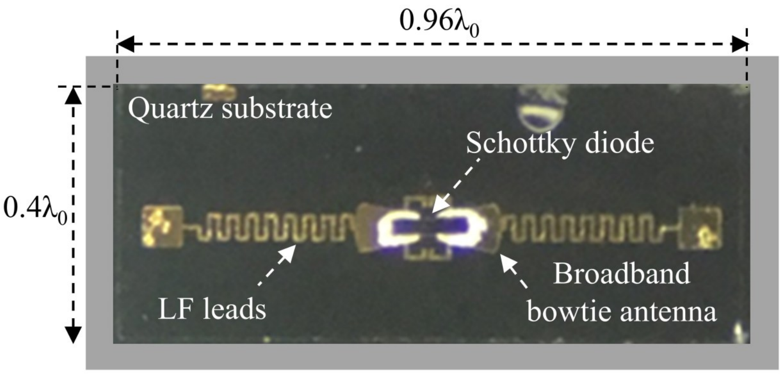

Fig. 10　Micrograph of fabricated quasi-optical detector chip
图10　制备完成的准光探测器芯片的显微照片

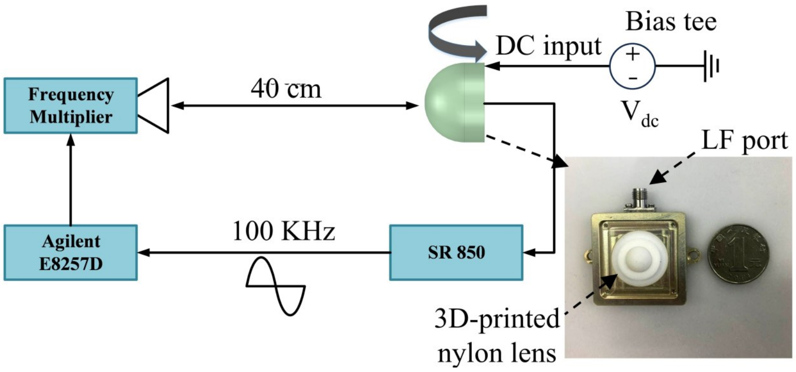

Fig. 11　Schematic diagram of the quasi-optical detector measurement setup, the inset shows the packaged detector module
图11　准光探测器测量系统的原理示意图，插图展示了封装后的探测器模块

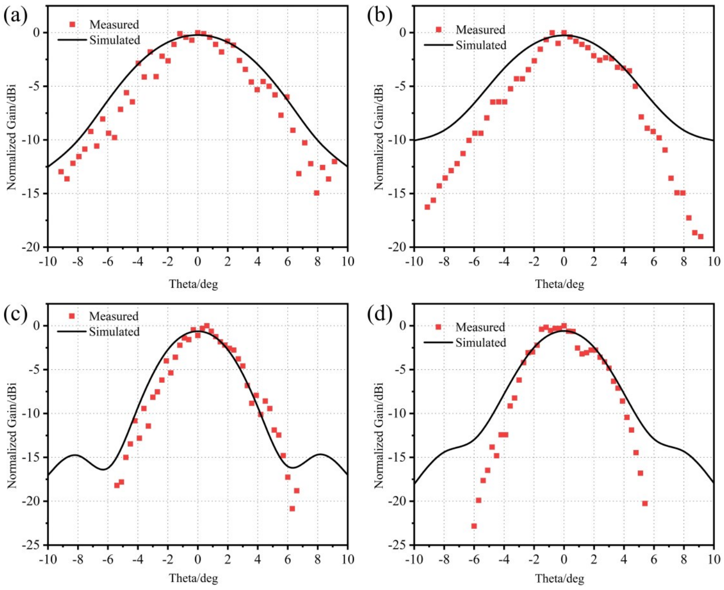

Fig. 12　Simulated and measured radiation patterns of the lens antenna at (a) 220 GHz, E-plane, :(b) 220 GHz, H-plane, (c) 340 GHz, E-plane, (d) 340 GHz, H-plane(b) 220 GHz, H-plane, (c) 340 GHz, E-plane, (d) 340 GHz, H-plane
图12　透镜天线在不同频率和平面下的仿真与测量方向图 (a) 220 GHz, E-plane,

na, antenna radiation characteristics, as well as various measurement and calibration errors[21]. Since the diode is directly integrated at the feeding port of the antenna, it becomes challenging to achieve efficient impedance matching between the diode and the antenna in the absence of an impedance matching network, while maintaining desirable radiation performance. In future work, we will focus on designing advanced antenna and circuit structures to realize efficient impedance matching and effective RF coupling. Additionally, efforts will be devoted to establishing accurate modeling and optimization methods to further enhance system performance.

The noise equivalent power (NEP) is also an important parameter for the quasi-optical detector, which can be evaluated by

$$NEP = \frac{V_N}{R_V} \qquad (4)$$

Where V_N is the thermal noise voltage spectral density of the detector that is mainly contributed by SBD. V_N can be obtained by

$$V_N = \sqrt{4kT(R_s + R_d)} \qquad (5)$$

Based on (4) and (5), and the measured NEP of the quasi-optical detector can is 1. 18-2. 53 pW/H$^{0.5}$ in the 200-230 GHz range and 1. 37-2. 51 pW/H$^{0.5}$ in the 320-350 GHz range. Table 1 summarizes the performance of the proposed quasi-optical detector in comparison with other SBD-based counterparts. The results indicate the proposed quasi-optical detector, distinguished by its lightweight design and mechanical robustness, performs betters than other forms of detector in terms of broad operational bandwidth and responsivity.

3 Conclusions

In this paper, a broadband quasi-optical detector operating from 201 to 360 GHz has been presented, featuring a lightweight 3D-printed lens. A bowtie antenna integrated with a pair of CLL is employed to extend the operational bandwidth without significantly altering the overall antenna dimensions. To achieve unidirectional radiation and gain enhancement, a 3D-printed lens is combined with a planar reflector embedded in a multi-layer substrate. Based on the integrated bowtie antenna and SBD, an antenna-coupled detector is fabricated and experimentally characterized. The measured responsivity ranges from 1025 to 2200 V/W in the 200-230 GHz range, corresponding to a NEP of 1. 18-2. 53 pW/H0. 5, and from 1033 to 1885 V/W in the 320-350 GHz range, corresponding to a NEP of 1. 37-2. 51 pW/H0. 5. These experimental results validate the proposed design, exhibiting huge potential in the sub-THz sensing and imaging applications.

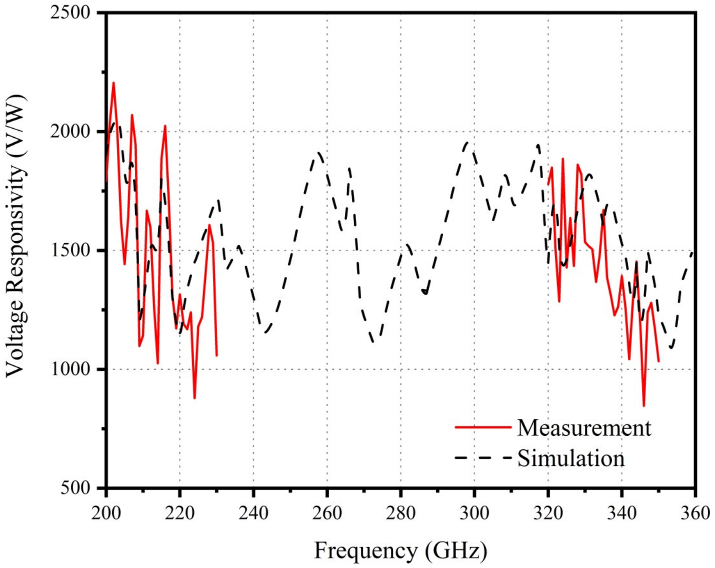

Fig. 13 Simulated and measured responsivity of the quasi-optical detector
图13 准光探测器的仿真与实测响应率

Table 1 Comparisons with other reported terahertz detectors
表1 与其他报道的太赫兹探测器对比

Ref.	Freq. /GHz	Gain component	Max. Resp. /(V/W)	SBD. Type technology
[7]	270–290	Reflector	250	CMOS Monolithic
[8]	75–170	Silicon Lens	800	GaAs Monolithic
[9]	140–240	Silicon Lens	280	GaAs Hybrid
[12]	150–440	Silicon Lens	1000	Zero bias
This work	201–360	3D-printed Lens+reflector	2200	GaAs Hybrid

References

［1］Nagatsuma T，Ducournau G，Renaud C C. Advances in terahertz communications accelerated by photonics ［J］. Nature Photonics，2016，10(6)：371-379.

［2］Wang C，Lu B，Lin C，et al. 0.34-THz wireless link based on high-order modulation for future wireless local area network applications ［J］. IEEE Transactions on Terahertz Science and Technology，2014，4(1)：75-85.

［3］Jasteh D，Hoare E G，Cherniakov M，et al. Experimental low-terahertz radar image analysis for automotive terrain sensing ［J］. IEEE Geoscience and Remote Sensing Letters，2016，13(4)：490-494.

［4］Qiu Y，Meng K，Wang W，et al. Efficient free-space to on-chip coupling of THz-bandwidth pulses for biomolecule fingerprint sensing ［J］. Optics Express，2023，31(2)：13.

［5］Hillger P，Grzyb J，Jain R，et al. Terahertz imaging and sensing applications with silicon-based technologies ［J］. IEEE Transactions on Terahertz Science and Technology，2019，9(1)：1-19.

［6］Cheng B，Cui Z，Lu B，et al. 340-GHz 3-D imaging radar with 4Tx-16Rx MIMO array ［J］. IEEE Transactions on Terahertz Science and Technology，2018，8(5)：509-519.

［7］Han R，Zhang Y，Coquillat D，et al. A 280-GHz Schottky diode detector in 130-nm digital CMOS ［J］. IEEE Journal of Solid-State Circuits，2011，46(11)：2602-2612.

［8］Zah C E，Kasilingam D，Smith J S，et al. Millimeter wave monolithic Schottky diode imaging arrays ［J］. International Journal of Infrared and Millimeter Waves，1985，6(10).

［9］Liu L，Xu H，Duan Y，et al. A 200 GHz Schottky diode quasi-optical detector based on folded dipole antenna［J］. 20th International Symposium on Space Terahertz Technology，2009：145 – 149.

［10］GUO Da-Lu，LV Xin，et al. A 2 × 2 integrated heterodyne receiver array for terahertz imaging application ［J］. //International Conference on Microwave and Millimeter Wave Technology Proceedings，2016：795 – 797.

［11］J. L. Hesler and T. W. Crowe. Responsivity and noise measurements of zero-bias Schottky diode detectors ［J］. 18th International Symposium on Space Terahertz Technology，2007：89 – 92.

［12］Liu L，Hesler J L，Xu H，et al. A broadband quasi-optical terahertz detector utilizing a zero bias Schottky diode ［J］. IEEE Microwave and Wireless Components Letters，2010，20(9)：504-506.

［13］Mou J，Xue Q，Guo D，et al. A THz detector chip with printed circular cavity as package and enhancement of antenna gain ［J］. IEEE Transactions on Antennas and Propagation，2016，64(4)：1242-1249.

［14］Tang M C，Chen Y，Ziolkowski R W. Experimentally validated，planar，wideband，electrically small，monopole filtennas based on capacitively loaded loop resonators ［J］. IEEE Transactions on Antennas and Propagation，2016，64(8)：3353-3360.

［15］Lin C C，Jin P，Ziolkowski R W. Single，dual and tri-band-notched ultrawideband （UWB） antennas using capacitively loaded loop （CLL） resonators ［J］. IEEE Transactions on Antennas and Propagation，2012，60(1)：102-109.

［16］Gorur A，Karpuz C，Akpinar M. A reduced-size dual-mode bandpass filter with capacitively loaded open-loop arms ［J］. IEEE Microwave and Wireless components letters，2003，13(9)：385-387.

［17］Guo Y，Zhou J. Total broadband transmission of microwaves through a subwavelength aperture by localized E-field coupling of split-ring resonators ［J］. Optics Express，2014，22(22)：27136-27143.

［18］Paolella A C，Fisher C D，Corey C，et al. 3-D printed millimeter-wave lens systems at 39 GHz ［J］. IEEE Microwave and Wireless Components Letters，2018，28(6)：1-3.

［19］Yi H，Qu S W，Ng K B，et al. 3-D printed millimeter-wave and terahertz lenses with fixed and frequency scanned beam ［J］. IEEE Transactions on Antennas and Propagation，2016，28(2)：442-449.

［20］Filipovic，D F，Gearhart，S S，Rebeiz，G M. Double-slot antennas on extended hemispherical and elliptical silicon dielectric lenses ［J］. IEEE Transactions on Microwave Theory and Techniques，1993，41 (10)：1738-1749.

［21］Mou J，Shen Z，Guo D，et al. Compact and wideband millimeter-wave antenna-coupled detector ［J］. IEEE Transactions on Microwave Theory and Techniques，2018，66(2)：1058-1069.